# Performance Assessment of Predictive Lane Boundary Detection for Non-uniformly Illuminated Roadway Driving Assistance

Avishek Parajuli, Mehmet Celenk, and H. Bryan Riley
School of Electrical Engineering and Computer Science
Stocker Center, Ohio University
Athens, Ohio 45701 USA
{ap356311, celenk, rileyh1}@ohio.edu

***Abstract* - In this paper, we focus on the performance of an earlier developed method for the detection of road lane markers which are minimally affected by non-uniform surface illumination (e.g., shadows and highlights) and road geometries. We investigate the detection performance and associated parameters of this approach. Experimental results show that the method yield accurate results in various situations such as broken or missing lane markings, the curved lane, the heavy shadows, the sun glare, and the occlusion of other vehicles. The accuracy and precision of the proposed model are presented and compared with existing methods as reported in the current literature. Specifically error curves are computed and presented for the actual verses predicted lane markers by blending salient features from the Gradient Spectrum Matching (GSM) and Principal Component Analysis (PCA) methods.**

***Keywords-component: Linear Prediction, Lane Marker Detection and Identification, Machine Vision, Information Fusion, Gradient Spectrum Matching, PCA, Driving Assistance Roadway Features***

## I. INTRODUCTION

The problem of accurate detection and localization of lane boundaries or lane markers is well investigated for Intelligent Transportation Systems (ITS) and self-driving autonomous vehicles. As the technical debate continues to loom regarding embedding intelligence in the infrastructure or directly into the vehicle for autonomous driving applications, the need to clearly delineate lane markings with a high degree of robustness and accuracy becomes even more essential. This is for safety and aiding detecting lane markers with accuracy for navigation systems. Currently, a significant number of computer vision based techniques are present in the literature for the detection and tracking of lane markings [1], [2]. Broadly speaking lane detection algorithms can be classified in two broad categories, namely, model or template based [3-8, 13] and feature based [9-12, 16-19, 28].

The template based lane detection algorithm has a predefined set of template lane models (linear, spline, parabola) for representing the road lanes. These algorithms typically preprocess the image and extract parameters to find the best model for the lane markings in the image from a predefined set of templates [4]-[6]. These methods give good result in detection of roads segments of various shapes during normal environmental condition. However, these template based methods are limited to structured road environments and are unable to perform well when weather and road surface conditions change since a finite number of templates can be generated from a practical standpoint to model a particular road scene. In [8], Yue et al. used the cubic B- spline to model the lane boundaries and presented the Canny Hough Estimation of Vanishing Point (CHEVP) algorithm for locating the initial points and locating the vanishing lane marker lines. This methods can detect lane markers in straight and curved road segments, however, it still reports false points in the presence of artifacts when shadows are casts by tree trunks, poles, and buildings onto roadway surfaces as indicated in [16], [21] .

In [9], [11], a feature based lane detection algorithm method is presented for the detection of road lane markings which employs edge detection and the Hough transform. These methods perform accurately for a given environment where the illumination is uniform but the performance degrades rapidly when the illumination changes and a new suitable intensity threshold is required to remove the unwanted edges. Borkar et al. presented a method [12], based upon edge detection, the Hough transform, and temporal characteristics for the purpose of real time lane detection during night-time. However, this method is heavily influenced by shadow and illumination conditions and is further limited for straight roadway segments. Additionally, these methods have experienced difficulties when choosing a suitable intensity threshold to remove the unwanted edges without degrading the true road lane marker edge points. Lane finding in another domain (LANA) [9] obtains information about the intensity and direction of the edges by using frequency domain features. However, performance of both methods in varying illumination conditions and over a wide variety of road shapes will be a critical issue to examine.

In this research work, we proceed to motivate a dual path processing algorithm primarily based on the GSM and the PCA, which does not require threshold for edge detection, or binary image conversion and report the significantly improved results in the form of error curves.

978-1-5090-2491-9/16 $31.00 © 2016 IEEE
DOI 10.1109/CRV.2016.52

## II. CURRENT LITERATURE AND MERIT OF RESEARCH

### A. Related Work Reported in the Literature

The following discussion summarizes various approaches and research results as reported in the current literature for lane marking detection and identification.

Wang et al. [18] proposed a method for lane detection and tracking which combines parabolic model and the Hough transform to detect both the straight and curved segments of the road. The method follows the traditional approach using the Prewitt edge operator followed by constant threshold to obtain a binary edge detected image. Afterwards the Hough transform is used for initial boundary detection followed by fitting of parabolic curve for lane boundary detection and tracking. As discussed in the results section of [18], the presence of large shadow leads to incorrect results, respectively.

Lipski, [13], formulated a data fusion algorithm (input from multiple cameras) and employed RANSAC (RANdom SAmple Consensus) algorithm to generate lane models using the feature points from the multiple cameras. While the method is robust and computationally efficient, it is limited to use in real time operations at low vehicle speeds. Also the presence of vehicles and other obstacles on the road leads to the detection of a large number of false lane points.

Sivaraman and Trivedi [15] presented a method for lane detection and tracking using vehicle localization where lane detection is performed by using steerable filters. Lanes are tracked by the Kalman filter and vehicle tracking is done using condensation particle filtering. They mainly focused on lane tracking in high density traffic scenes and it tends not to perform well in low traffic conditions where there is no vehicle ahead of the host vehicle. Furthermore, the Kalman filter is computationally more expensive than the Yule-Walker predictor [22].

The authors in [25] presented an excellent algorithm for extraction of single pixel width lane edge that uses dynamic left and right threshold values along each row of the image. The presented method has advantages to the existing feature-based lane detection, which uses the Canny, Sobel edge enhancements followed by thresholding and the Hough transform, in terms of being independent to illumination condition and threshold values. It experiences a tradeoff in that the inherent design has suboptimal performance in conditions where occlusion of adjacent vehicles, diminished or missing road lane markers, worn out road conditions, and presence of road construction materials occur.

In [26], authors present another well-known algorithm that starts with the trends of edge enhancement followed by binarization (threshold value of 0.6) and application of the Hough transform. While the authors claim that method is suitable for real-time applications, and robust to shadows, weather condition and illumination, the latter is challenging because it employs constant threshold values for all the different ranges of images. Also, in case of diminished lane markers, these methods can be improved by incorporating a feedback channel that utilizes the previous results in current calculations.

Gaikwad et al. [27] uses a piecewise linear stretching function (PLSF) to divide the road into five different sub regions based upon the gray value intensity levels. Here, the authors claimed a 97% achievement in accuracy of lane departure identification (i.e., not lane detection) over the chosen database, the lane detection method used has a serious drawback of not being able to perform well over high dynamic image intensities, and non-uniform surface illumination. This is due to the fact that the PSLF assumes that image intensities below 0.45 are roadway surfaces, and image intensities above 0.75 corresponds to lane markers, which is an invalid assumption for all illumination conditions.

Chang et al. in [28], have presented an algorithm based on adaptive thresholding and Hough transform to fit lane markers as straight line segments that can detect lane markers in real-time conditions for various conditions. This method is efficient, suitable for real-time application but the detection results are limited to the near field of the image which are usually straight. Even though the author claims the method to work on complex shadows, the complexity of images subpar to the image datasets [20] employed herein.

Fan et al. [16] proposed a new method for lane detection and tracking which uses the angle component of the gradient to compute the Edge Distribution Function (EDF), Hough transform and bi-directional sliding window. Their results yielded 94% successful rate when tested on the image dataset [20]. However, it is challenging to conclude their proposed method can track the curved sections of the road in the far field of the image with heavy shadows, and the diminished road lane markers as evident by the results. Also, the authors fail to provide quantitative analysis of the accuracy obtained and selectively state the number of successfully detected images.

Parajuli et al. [19] proposed a new method for lane detection which uses the frequency domain features of the lane markings. Simulation results yield a 95% successful rate using the images from [20]. Upon review of the algorithm's performance with this specific data set we note the drawback of high false alarms. Additionally the authors left open an opportunity to provide a quantitative analysis of the accuracy obtained.

The authors in [17] have put forward a method to perform High Dynamic Range (HDR) lane detection and tracking system that is robust in varying conditions of illumination. Kou et al. [17] begins with obtaining HDR image by merging three images with varying exposure rates from a single camera. Then, the HDR image is processed to detect lane boundaries whose accuracy would not be affected by lightning conditions. The authors assert that the computation time achieved by their method is 65 ms, which is better than that of others and can be used for real time

applications. However, no information has been provided on the number of images used for the testing. The method can be robust and computationally efficient over a varying condition of lighting but most of the detection results presented were only straight road line segments. Therefore, there is a need for a method that works on varying illumination conditions as well as for straight and curved segment of the road. These problems are addressed and a method is presented for lane detection and tracking irrespective of the presence or absence of on-road vehicles. We employ PCA to determine the direction of the lane markers within the local window selected on the lane markers. Additionally, the ARMA (Auto Regressive Moving Average) model based Yule-Walker regression successfully predicts the direction of lane markers with a high degree of accuracy [22].

### B. *Contributions of the Current Research Work*

The merit of this research is twofold. First, we introduce an imperative information selection method that merges the data from the GSM [19] and PCA method, thereby reducing uncertainty. Second a performance assessment and comparison of existing methods will distinctly show the proposed algorithm exhibits improved accuracy of the lane detection on roadways with non-uniform surface illumination. To that end, our proposed method yielded true detection rate of approximately 97% over a public databases of images which is higher than the existing literature [8], [13], [16], [18], and [19]. Compelling results are computed, presented and described, respectively. The present work is different than [19] as it introduces the application of PCA to detect the lane markers and provides improved detection accuracy.

## III. Description of the Method

A high-level functional flow chart is shown below in Figure 1 and it depicts the functional flow for the algorithm. The process begins with extraction of individual frames of the video and processing each single image frame to detect the lane markers or lane boundaries from the database in [20]. The first step is the conversion of the RGB image into a grayscale image. The gray scale image is fed into the gradient spectrum method [19] which extracts the vertical edges of the image to remove the effect of shadows that are generally horizontal. The first few points detected by the GSM method are used to initialize the principal component analysis (PCA) subroutine [24]. After the initialization of PCA subroutine, the PCA method works to compute the direction of lane and follows the lane markings along the road. The PCA subroutine operates in the spatial space by computing major direction (principal component) of the grayscale image. This is within a local window placed on the lane markings whereas the next lane points on the next horizontal line and is computed by using the major direction vector (see Figure 2). The information selection algorithm uses the results of the GSM and PCA methods. The latter stages of the algorithm then combine the results to reduce the uncertainty of the lane markers.

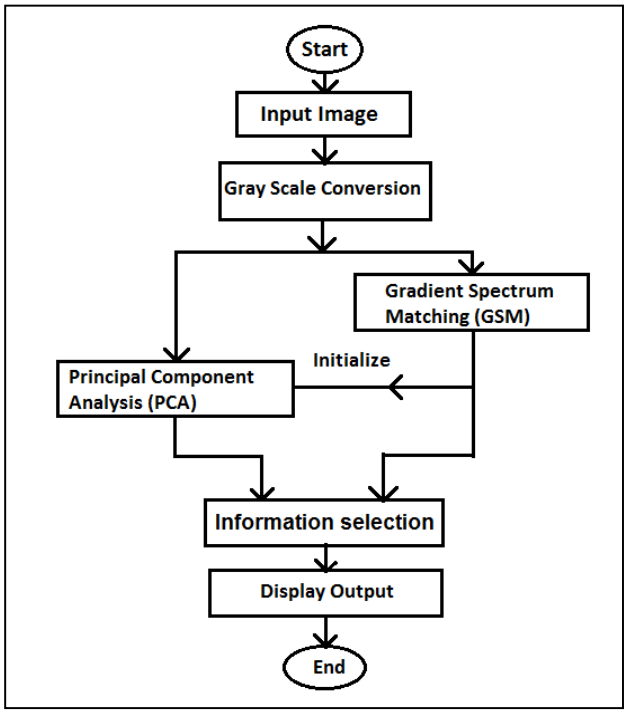


Figure 1: High level functional flow chart

### A. *Gradient Spectrum Matching Method (GSM)*

The GSM method incorporates frequency domain features of the lane markings and the gradient spectrum matching function as outlined in author's previous work [19]. This method generates characteristic left, and right lane features i.e., gradient spectrum magnitude within a local window, for left and right lane markers, respectively from a set of training data images as, respectively. The precisely localized lane points along the horizontal scan line are obtained on the test image by using the normalized cross-correlation between the generated gradient spectrum and the baseline characteristic left and right lane spectra. The lane points obtained from the GSM method are used later in the information selection stage to compare with the data from PCA.

### B. *Principal Component Analysis Method (PCA)*

The PCA [24] subroutine executes in the spatial space by computing major direction (eigenvector) of the grayscale image within the local window placed on the lane markings. The PCA based lane detection method does require initial information about the localization of right, and left lane points. This initial information of lane points is provided by the GSM method. The first three left and right lane points on the horizontal scan line detected by the GSM is provided as initial points to the PCA unit. After the initialization process, the PCA module is independent of the GSM method and both these methods work in parallel and independent of each other. The local window's major axis orientation (eigenvector) determines the direction of the road lane markers and is updated to the next scan line along the direction of previous eigenvectors. The next horizontal scan

line is at a distance of five pixel points from the current horizontal scan line.

Consider the diagram of Figure 2 as it depicts a roadway surface with lane marking on each side of the path. Also, consider a horizontal scan line that intersects the left and right lane markers at points L, and R, respectively. Initially, the points L and R are provided by the GSM method during the initialization step as shown in Figure 2. A local window of size 15x15 is placed at the points L and R. The local windows' major axis orientation is computed at points L and R on the horizontal scan line. The lane points on the next scan line are calculated in the direction of the window's major axis orientation from the preceding scan lines. In other words, the lane markers direction from current scan line generates the lane markers points on the next scan line. This process continues along the lane markers until the lane markers are obstructed by some objects (outliers) or end of the image. The progressive lane markings points are drawn on the horizontal scan line based on the PCA major axis orientation changes.

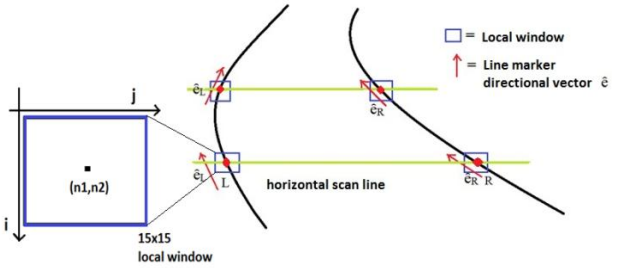


Figure 2: Schematic representation of the two lane road with lane markers, local window and line markers unit directional vector

*1) Local window size*

The dimension of the local window is non-trivial and was selected as 15x15 after an extensive experimentation on a large number of images. A window of this dimension was determined to produce the most consistent and accurate representation of the lane markers' direction (major axis orientation) from the PCA. Table 1 presents the results from various dimension sizes.

**Table 1: Results for varying window size**

| | |
|---|---|
| 5x5 | Varying results |
| 7x7 | Varying results |
| 11x11 | Varying results in different images |
| 13x13 | Invariant to translation, rotation and scaling |
| 15x15 | Most invariant to translation, rotation and scaling |
| 17x17 | Varying results |

*2) Calculation of mean position vector and covariance matrix*

In Figure 2, the horizontal scan line intersects the left lane marker at point L. Let the co-ordinates of the image $G$ at point L be $(n_1, n_2)$ where $n_1$ is the row number and $n_2$ is the column number of the image. A 15x15 local-window is placed such that the center of the window is at$(n_1, n_2)$. If **A** is the matrix containing the pixel points within the local window we now have **A** defined as:

$$\mathrm{A} = G(n_1 + k, n_2 + l) \quad \forall \ -7 \le k \le 7 \ , -7 \le l \le 7; \tag{1}$$

where $k$, $l$ take discrete values -7, -6,…, 0,…, 6, 7.

Using matrix and vector notation, the 15x15 matrix A can be written as

$$\mathbf{A} = \begin{bmatrix} a(1,1) & \cdots & a(1,15) \\ \vdots & \ddots\ a(8,8) & \vdots \\ a(15,1) & \cdots & a(15,15) \end{bmatrix} = \begin{bmatrix} G(n_1-7, n_2-7) & \cdots & G(n_1-7, n_2+7) \\ \vdots & \ddots\ G(n_1, n_2) & \vdots \\ G(n_1+7, n_2-7) & \cdots & G(n_1+7, n_2+7) \end{bmatrix} \tag{2}$$

The elements of matrix **A** can be generalized as

$$a(i,j) = G(n_1 + i - 8, n_2 + j - 8) \tag{3}$$

where i, j = 1, 2… 15.

$G(n_1, n_2)$ is the center pixel on which the local window is positioned (see Figure 2 insert above), and $n_1, n_2$ are the row column numbers respectively of the center pixel.

The mean vector ($\vec{u}$) for the matrix **A** is computed by using the equation (4) given below

$$\vec{u} = \frac{1}{\sum_i \sum_j a(i,j)} \sum_{i=1}^{15} \sum_{j=1}^{15} \vec{X} \cdot a(i,j) \tag{4}$$

where $\vec{X} = \begin{bmatrix} i \\ j \end{bmatrix}$ is the position vector.

The covariance matrix $\boldsymbol{C}$ for the matrix **A** is computed as represented in (5)

$$\mathbf{C} = \frac{1}{\sum_i \sum_j a(i,j)} \sum_{i=1}^{15} \sum_{j=1}^{15} \vec{X} \cdot \vec{X}^T \cdot a(i,j) - \vec{u} \cdot \vec{u}^T \tag{5}$$

*3) Calculation of eigen vector (principal component)*

Let $\vec{e}$ be the eigenvectors of the matrix $\boldsymbol{C}$ such that

$$(C - \lambda I) \cdot \vec{e} = 0 \tag{6}$$

where $\lambda$ is the eigen value, and $I$ is the 2x2 identity matrix.

The eigenvectors $\vec{e}$ can be computed from (7) as follows:

$$C \cdot \vec{e} = \lambda \cdot \vec{e} \tag{7}$$

Since the eigenvector corresponding to the eigen value with maximum magnitude is the principal component [31] or the local window's major orientation which depicts the

direction of the lane markings. The principal component vector is $\vec{e}$ when

$$\lambda = \lambda_{max} = \max(\lambda_1, \lambda_2) \quad (8)$$

where $\lambda_1$, $\lambda_2$ are two eigenvalues obtained from equations (6) and (7), respectively.

*4) ARMA model Yule Walker prediction*

The horizontal scan line intersects with the lane markers (see Figure 2) at points L, R on left, and right lane markers respectively. At each point L and R on the horizontal scan line following the computational process proceeds as follows:

i. At points L, R the 15x15 local window is positioned and we compute the largest eigen-values ($\lambda_L$ and $\lambda_R$) and unit eigenvectors ( $\hat{e}_L$ and $\hat{e}_R$ ) from the PCA analysis, respectively.

ii. Representaion of those vectors from PCA are in the form of

$$\hat{e}_L = |\hat{e}_L| \angle \theta_L \quad (9)$$
$$\hat{e}_R = |\hat{e}_R| \angle \theta_R \quad (10)$$

iii. Compute the lane marker (i.e., prediction)

The Yule-Walker equation of second degree is used to predict the lane direction. The block diagram of this prediction process is provided in Figure 3 and the equations (11) and (12) mathematically model and predict the forward direction of the lane markers.

$$\hat{\theta}_L(n+1) = \alpha_1 \theta_L'(n) + \alpha_2 \theta_L'(n-1) \quad (11)$$
$$\hat{\theta}_R(n+1) = \beta_1 \theta_R'(n) + \beta_2 \theta_R'(n-1) \quad (12)$$

where $\hat{\theta}_L$, $\hat{\theta}_R$ are the predicted road directions; $\theta_L'$ and $\theta_R'$ are the corrected directions, and $\theta_L(n)$, $\theta_R(n)$ are the actual calculated direction at discrete time n.

The variables, $\alpha_1$, $\alpha_2$, $\beta_2$, and $\beta_2$ are the 2nd order ARMA coefficients are calculated as described in [22].

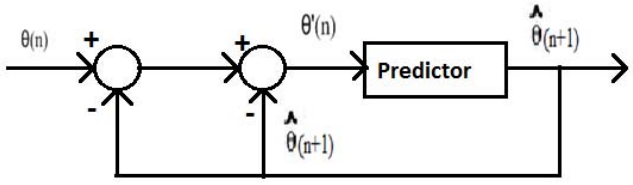


Figure 3: Block diagram for ARMA model predictor

*C. Imperative Information Selection*

Earlier discussions indicated, the image sequence is processed in parallel by two methods namely the gradient spectrum matching (GSM) method, and the Principal Component Analysis (PCA) method. The lane points detected by these two methods are then plotted on the original RGB image and shown in Figure 5. The detected lane points are now input data for the prediction module, thereby producing a cluster of points along the right and left lane markings. The inherent nature of the information algorithm allows for the selection of the best left and right lane marking points along each scan line from the four different available points (i.e., predicted, calculated points from both the PCA and GSM methods). The selection of this vital information is based upon the principle of Least Square Error (LSE) criterion [24] which minimizes the error between the detected and the predicted points.

The block diagram in Figure 4 presents the working principle of the information selection process. Let $g_L(n)$ and $\widehat{g_L}(n)$ be the detected and predicted left lane marking points by the GSM method at n$^{th}$ horizontal scan line and $\xi_1(n)$ is the error between the detected and predicted points is given by equation (13).

$$\xi_1(n) = g_L(n) - \widehat{g_L}(n) \quad (13)$$

Similarly, $p_L(n)$ and $\widehat{p_L}(n)$ be the detected and predicted left lane marking points by the PCA method at the n$^{th}$ horizontal scan line. The error between the PCA predicted and detected points is $\xi_2(n)$ and represented by equation (14) as

$$\xi_2(n) = p_L(n) - \widehat{p_L}(n) \quad (14)$$

The Least Square Error (LSE) criterion is used to choose the left and right points along each horizontal line. This is represented in equation (15).

$$y_L(n) = \widehat{p_L}(n), \text{ given } \xi_2(n)^2 < \xi_1(n)^2$$
$$= \widehat{g_L}(n), \text{ given } \xi_2(n)^2 > \xi_1(n)^2 \quad (15)$$

where n is the n$^{th}$ scan line, starting from the bottom of the image; n=1, 2, 3…,N.

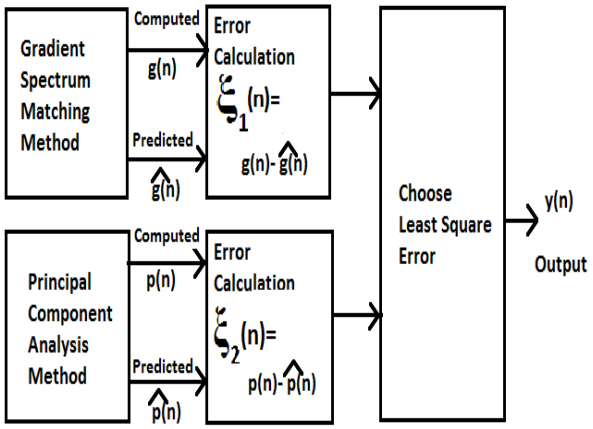


Figure 4: Imperative information selection flowchart

This process is applied to both for left and right lane points for each horizontal scan line, and the best lane point is stored in $y(n)$. It is important to note that $y(n)$ contains the

column number of the optimum left and right points for the $n^{th}$ horizontal scan line, while the row number at each point on the given horizontal scan line is constant and predefined. The choice of the optimum points from equation (15) leads to increased accuracy and improved results for the lane detection as seen below in Figure 5, which signifies the predictive detection accuracy.

Figure 5 shows the result of GSM, and PCA method along with the horizontal scan line on the top left and middle column as indicated. The top right column is the result obtained after the imperative information is selected from the two methods (PCA and GSM). The computed and predicted points for left and right lane markings on each horizontal scan line (n) are plotted in Figure 5 for both the PCA and GSM method. The error between the prediction and computed points is computed and as shown in the Figure 5. The predicted points, corresponding to the minimum error in a mean square sense between the PCA and GSM method. The results are selected for each horizontal scan line per the computations and shown in Final Result below.

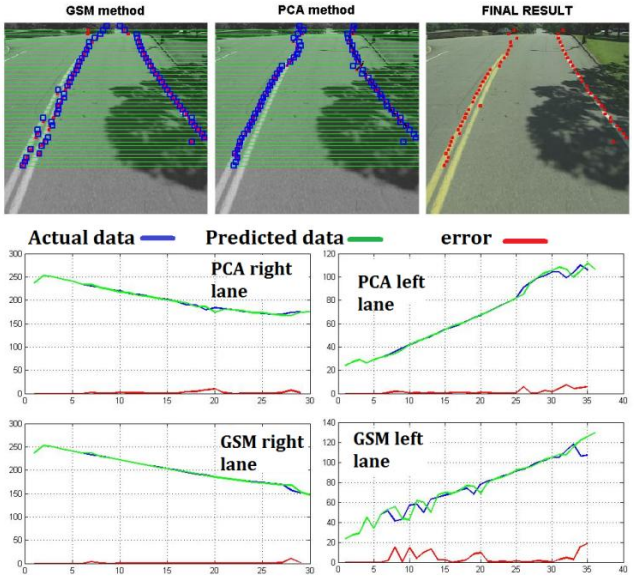


Figure 5: Results of the GSM method, PCA method and information selection and the respective error curves on lane segments. The red, blue points on the image results from GSM and PCA method are detected and predicted points respectively. The final image containing red points are the final result from the relevant information based upon the error curves. The error curves are plotted as a function of column no Vs horizontal scan line number, n.

## IV. Experiment and Results

### A. Experimental Setup

A quantitative evaluation of our proposed lane marker detection algorithm and corresponding results are now presented. The algorithm is coded and is tested utilizing images from an open source database [20] commonly used for various experimental imaging investigations. The dataset [20] consists of 157 images of sunny-1 lane road with different variety of road conditions such as straight lanes, curved lanes, and occlusion of lane by vehicles, missing lane markings, shadows, and non-uniform surface illumination. The GSM method, PCA method, and the information selection algorithms were implemented in MATLAB 2008 and executed on a PC with a clock rate of 2.2 GHZ.

### B. Results

The primary focus is on the accuracy of lane marker detection by looking at the true positive rate against the false positive rate for different diagnostic test runs of the road images. The error is presented as Receiver Operating Cures (ROCs) with the intent to depict the tradeoff between sensitivity and specificity inherent in each roadway image tested. First tests images were manually visualized and the lane points detected in a trailing image after information selection process. Next the approach consisted to labeling them either as correctly detected, false lane points, or misses. For some image conditions the algorithm detects a lane point which is present on the lane, it records correct detection or true positive (TP). For other image conditions the algorithm fails to detect a lane point, and records the result as a miss. Yet in other conditions if algorithm detects a non-lane point as a lane point, the algorithm reports the detection as a false alarm.

This approach is robust and performs well independent of significant variation among the images in the selected database. The presence of artifacts such as shadows, non-uniform illumination condition, diminishing or missing lane markers, and high dynamic illumination ranges inherently makes lane detection difficult on these road images. Table 2, presents the algorithm performance data for total lane points, number of correctly detected lane points, and number of misses. The detection rate for the lane markers points was computed to be 97.39%. The majority of results depicted in Figure 6 and Figure 7 are the images of adverse scenarios and justifies the promise of this approach.

**Table 2: Lane detection results on the CMU/VASC dataset [20]**

| | |
|---|---|
| Total images | 157 |
| Total no of true lane points | 10022 |
| Number of correctly detected lane points, true positive(TP) | 9761 |
| Number of incorrect detection | 261 |
| Number of false alarms | 261 |
| Number of misses | 291 |
| Detection accuracy | 97.39% |
| False alarm rate | 2.60% |
| Miss rate | 2.63% |

### C. Comparision of Performance

The algorithm presented herein, is tested on the publicly available image data bases [20]. The algorithm obtained successful detection rate of 97.39%. The detection accuracy of the presented algorithm is higher in comparison to the ones presented in [8], [16], [18], and [19].

**Table 3: Comparison of detection accuracy**

| Methods | Detection Accuracy |
|---|---|
| Wang et al. [8] | 95% |
| Fan et al. [16] | 94% |
| Parajuli et al.[19] | 95.54% |
| Proposed | 97.39% |

The algorithms presented in [8] [16], [19] use the same image database [20] as utilized by this research work. Clearly, this research work yields better performance than the existing methods presents in the literature. Moreover, the methods in [8], [16] and [19] present the accuracy results without the quantitative analysis of the process for obtaining the accuracy. This work evaluates the performance of the proposed algorithm through quantitative data analysis.

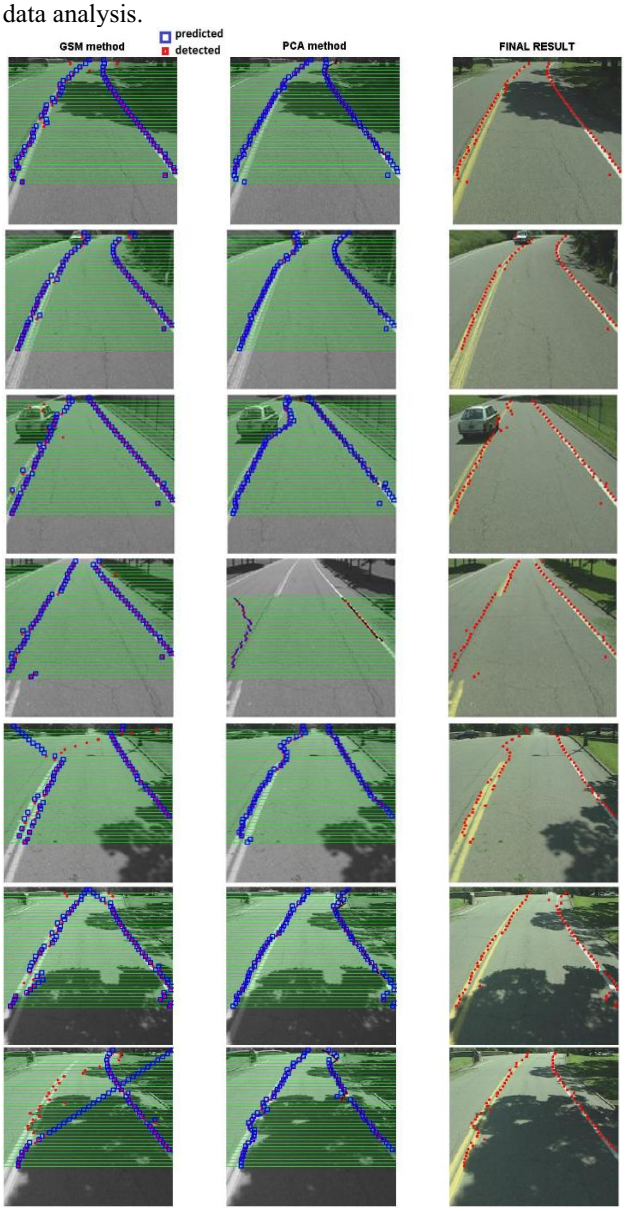


Figure 6: Results demonstrating advantage of information fusion (right column) over a variety of images with vehicles occlusion, straight, and curved road segments, shadows and missing lane markings.

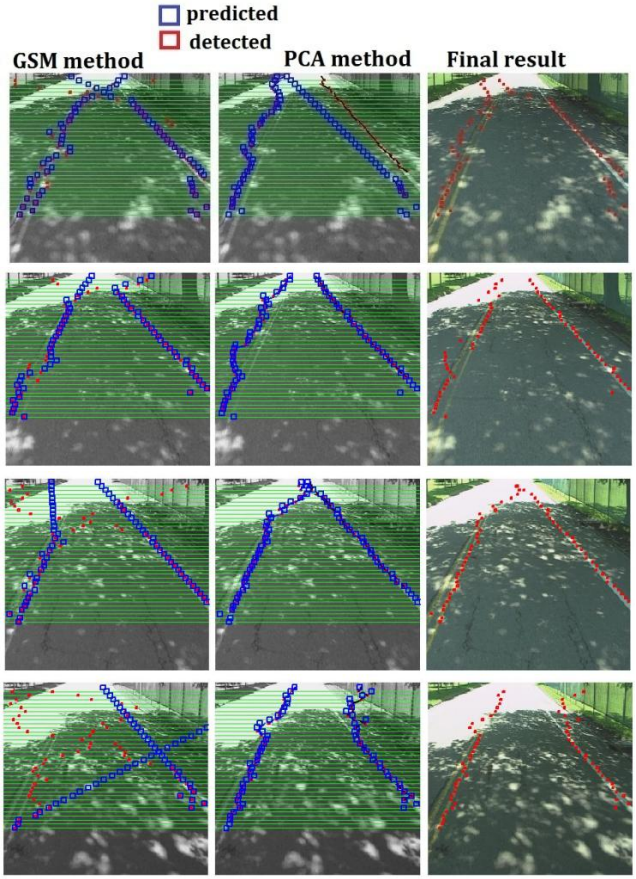


Figure 7: Final results (right column) in images with high dynamic illumination range and high non-uniform road surface illumination conditions.

Additionally, we have collected road images of various scenarios here in the Midwest USA using a commercial camera, and used this data as another source to evaluate our proposed algorithm with a detection rate of 97% over a variety of 1000 images. However, we cannot compare the performance of the proposed algorithm evaluated on locally obtained image data-sets against [16], [19] which are using different data-sets of images to evaluate performance. Therefore, we are limiting the comparison to the dataset [20].

## V. CONCLUSIONS

This research work has presented a rigorous and comprehensive data driven performance assessment of our earlier developed algorithm for the detection of lane markings in the presence of artifact such as shadows, non-uniform illumination conditions [19].We examine the performance in the presence of diminishing or missing lane markers, and high dynamic range images where only the intensity image spectra attributes are examined. The detection accuracy was shown to be several percentage points better than other approaches published in the current

literature. The experimental result obtained by testing the image database further supports the efficacy of the algorithm relative to others reported in the current literature and a study of the CPU usage and comparative processing times would be of interest to determine. Lastly it would be of great interest to apply this algorithm for detection of lane boundaries during heavy snowfall, unstructured roads and other inclement weather conditions.

## REFERENCES


[1] J. C. McCall and M. M. Trivedi, "Video-based lane estimation and tracking for driver assistance: survey, system, and evaluation," IEEE Transactions on Intelligent Transportation Systems, vol. 7, no. 1, pp. 20–37, 2006.

[2] A. Bar Hillel, R. Lerner, D. Levi, and G. Raz, "Recent progress in road and lane detection: a survey," Machine Vision and Applications, Feb. 2012, pp. 1-19.

[3] N. El Faouzi, H. Leung, and A. Kurian, "Data fusion in intelligent transportation systems: progress and challenges - A survey," *Information Fusion*, vol. 12, no. 1, pp. 4-10, Jan. 2011.

[4] K. Kluge, and S. Lakshmanan, "A deformable-template approach to lane detection," *Proceedings of the Intelligent Vehicles '95 Symposium*, Detroit, MI, pp. 54-59, Sept. 1995.

[5] D. Kang and M. Jung, "Road lane segmentation using dynamic programming for active safety vehicles," *Pattern Recognition Letters*, vol. 24, pp. 3177-3185, July 2003.

[6] S. Liou, and R.C. Jain, "Road following using vanishing points," in *Proceedings Computer Vision, Graphics, and Image Processing*, pp. 116-130, 1987.

[7] S. Lakshmanan and K. Kluge, "LOIS: A real-time lane detection algorithm," in *Proceedings 30th Annual Conference of Information Science Systems*, 1996, pp.1007–1012.

[8] Y. Wang, E. Teoh, and D. Shen, "Lane detection and tracking using B-Snake." Image and Vision computing, April 2004, vol. 22, no. 4, pp. 269-280.

[9] C. Kreucher and S. Lakshmanan, "LANA: A lane extraction algorithm that uses frequency domain features," *IEEE Transactions on Robotics and Automation*, Dearborn, MI, vol. 15, no. 2, pp.343-350, April 1999.

[10] J. McDonald, "Detecting and tracking road markings using the Hough transform," In *Proc. of the Irish Machine Vision and Image Processing Conference*, pp. 1-9. 2001.

[11] P. L. Palmer, J. Kittler, and M. Petrou, "An optimizing line finder using a Hough transform algorithm," *Computer Vision and Image Understanding*, vol. 68, no 1, pp. 1-23, July 1993.

[12] A. Borkar et al., "A layered approach to robust lane detection at night," in *Computational Intelligence in Vehicles and Vehicular Systems, 2009, CIVVS'09.,* Nashville, TN, pp. 51-57, May 2009.

[13] C. Lipski et al., "A fast and robust approach to lane marking detection and lane tracking," in *proceedings of IEEE SSIAI*, Santa Fe, NM, pp. 57-60, march 2008.

[14] C. Rasmussen, " Grouping dominant structure of Ill structured road following, " in *proceedings of IEEE computer society, CVPR 2004* , pp. I-470 - I-477 Vol.1, 27 June-2 July 2004.

[15] S. Sivaraman, and M. Trivedi, "Improved vision-based lane tracker performance using vehicle localization," in *Proceedings of IEEE intelligent vehicles symposium*, June 21-24, 2010.

[16] Y. Fan, W. Zhang, X. Li, L. Zhang, and Z. Cheng "A robust lane boundaries detection algorithm based on gradient distribution features," *Proceedings of the 8th International conference on Fuzzy Systems and Knowledge Discovery (FSKD)*, pp. 1714-1718, July 2011.

[17] F. Kou et al., "A lane boundaries detection method based on high dynamic range image," in *Proceedings of the 10th IEEE, International conference on Industrial informatics*, pp. 21-25, 2012.

[18] J. Wang, F. Gu, C. Zhang, and G. Zhang, "Lane boundary detection based on parabola method," in *Proceedings of the 2010 IEEE, International conference on Information and Automation*, pp. 1729-1734, china, June 2010.

[19] A. Parajuli, M. Celenk, and H. Riley, "Robust lane detection in shadows and low illumination conditions using local gradient features," *Open Journal of Applied Sciences*, Vol. 3 No. 1B, 2013, pp. 68-74. doi: 10.4236/ojapps.2013.31B014.

[20] Carnegie-Mellon-University, "CMU/VASC image database 1997–2003," http://vasc.ri.cmu.edu/idb/html/road/may30_90/

[21] Ju-Y. Kim et al.," A simple model for a lane detection system," in *Proceedings of Electronic Imaging and Signal Processing,* Feb. 2012.

[22] B. Porat, Digital Processing of Random Signals Theory and Methods. Englewood Cliffs, NJ: Prentice-Hall, 1994.

[23] J.S. Lim, Two Dimensional Signal and Image Processing, Prentice Hall 1990.

[24] S. Theodoridis and K. Koutroumbas, *Pattern Recognition*, 3rd Ed. New York: Academic, Feb. 2006.

[25] J. C. Cao, Q. H. Lin, and M. Y. Fu, "Extraction of single-pixel-width single edge using dynamic thresholding for lane detection on structured roads," IEEE China Summit and International Conference on Signal and Information Processing (ChinaSIP2014), Xi'an, China, pp.460-464, 2014.

[26] F. Sebdani and H. Pourghassem, "Robust and real-time road line extraction algorithm using Hough transform in intelligent transportation system application," IEEE Int. Conf. on Computer Science and Automation Engineering (CSAE), pp.256-260, 2012

[27] V. Gaikwad and S. Lokhande, "Lane departure identification for advanced driving assistance," IEEE Trans. on ITS, Issue:99, pp.1-9, Sept. 2014

[28] C. Chang et al., "An efficient method for lane-mark extraction in complex conditions," Ubiquitous Intelligence & Computing and 9th International Conference on Autonomic & Trusted Computing (UIC/ATC), *IEEE*, pp. 330-336, Sept. 2012.